Abstract. Detailed neutral hydrogen observations have been obtained of the large barred spiral galaxy NGC 3992 and its three small companion spiral galaxies, UGC 6923, UGC 6940, and UGC 6969. Contrary to the large galaxy, for the companions the H I distribution ends quite abruptly at the optical edges. Velocity fields have been constructed from which rotation curves have been derived. Assuming a reasonable M/L ratio, a decomposition of these rotation curves generates nearly equal dark matter halos. When comparing the position-velocity diagrams of the two brightest galaxies, UGC 6923 and UGC 6969, it is obvious that the rotation curve of the latter has a shape closer to solid body than the former, yet the same maximum rotational level is reached. This is likely generated by the equal dark matter halos in combination with UGC 6923 being a factor five more luminous than UGC 6969 and so its luminous matter gives a higher contribution to the rotation in the inner regions. An NFW-CDMΛ dark halo is consistent with the observed rotation curve of UGC 6923 but not consistent with the rotation curve of UGC 6969. If the NGC 3992 group is part of the Ursa Major cluster, then the I-band M/L ratio of NGC 3992 has to be at least 1.35 times as large as that of the average spiral galaxy in the cluster. On the other hand, equal M/L ratios can be achieved when the NGC 3992 group is placed more than 3 Mpc behind the cluster. Both possibilities can explain why NGC 3992 appears to be 0.43 magnitudes too faint for its rotation.

Key words: galaxies: individual: NGC 3992, UGC 6923, UGC 6940, UGC 6969 – galaxies: kinematics and dynamics – galaxies: interactions

A&A manuscript no.
(will be inserted by hand later)

Your thesaurus codes are:
missing; you have not inserted them

ASTRONOMY AND ASTROPHYSICS

Dark and luminous matter in the NGC 3992 group of galaxies

II. The dwarf companions UGC 6923, UGC 6940, UGC 6969, and the Tully-Fisher relation

Roelof Bottema

Kapteyn Astronomical Institute, P.O. Box 800, NL-9700 AV Groningen, The Netherlands, e-mail:robot@astro.rug.nl

Received date1; accepted date2

1. Introduction

Rotation curves derived from neutral hydrogen observations at the outer regions of spiral galaxies unambiguously show that substantial amounts of dark matter are required (Bosma 1978; Begeman 1987, 1989). Any physically reasonable distribution of this dark matter necessitates the presence of at least some of that in the inner optical disc region, contributing in some degree to the total rotation in that region. Unfortunately, from the observed rotation curve and light distribution one cannot a priori determine the ratio of dark to luminous matter (van Albada et al. 1985). There are arguments, mainly theoretical, that the contribution of the disc has to be maximized, leading to the so called maximum disc hypothesis (van Albada & Sancisi 1986; Sellwood & Moore 1999). On the other hand, observations of disc stellar velocity dispersions (Bottema 1993, 1997) lead to the conclusion that the disc contributes, on average, 63% to the total rotation at the position where the disc has its maximum rotation. This finding is supported by a statistical analysis of rotation curve shapes in relation to the compactness of discs (Courteau & Rix 1999). If the rotation is not measured outside the optical disc, the observed rotation curve can in most cases be explained by the stellar components alone (Kalnajs 1983; Kent 1986). This statement is valid for normal, medium and large galaxies. However, for smaller less massive or for galaxies with lower surface brightness, one does need dark matter already within the optical disc (Salucci et al. 1991; de Blok & McGaugh 1997). This indicates that small galaxies hold clear clues as to the size and shape of dark halos.

For a long time dark halos have been described by a pseudo isothermal sphere (Carignan & Freeman 1985). Such a halo has a constant density core and its rotation curve is characterized by two parameters. Numerical calculations of structure formation in a cold dark matter (CDM) dominated universe generate a different dark halo (Navarro et al. 1996, 1997). It has a central cusp where the density goes like r^{-1}. When a certain cosmology is chosen the structural scale is related to the total mass. Rotation curves are then characterized by only one parameter and are as such less flexible than rotation curves of isothermal halos. These halos are commonly referred to as NFW halos and seem to be able to fit the observed rotation curves of normal galaxies just as well (Navarro 1998). There is, however, quite some debate whether NFW halos can also fit the rotation curves of low surface brightness (hereafter LSB) galaxies.

At least when measured in kpc, rotation curves of LSB galaxies seem to rise slower in the inner regions than those of normal galaxies with the same luminosity (de Blok & McGaugh 1997; Pickering et al. 1997). That implies that for LSB systems the stellar disc can nowhere be dominant. If a disc is forced to its maximum contribution that leads in general to an excessively large mass-to-light ratio, while it is expected on the basis of colours and of metallicity that LSB galaxies have rather low M/L ratios. The establishment of slowly rising rotation curves of LSB galaxies is based on H I line observations. On the other hand, additional observations in the Hα line by Swaters et al. (2000) showed that in some cases beam smearing may have caused the H I rotation curves to be shallower than in reality. NFW halos cannot be reconciled with slowly rising, solid body rotation curves because for an r^{-1} density profile one has an $r^{1/2}$ rotation curve. For that reason it is rather important to establish the exact rotational behaviour of LSB galaxies in their inner regions. The structure formation calculations generate NFW halos on all linear scales. Therefore, if there is a class of objects for which NFW halos do not apply the CDM paradigm might be in serious trouble. In a recent paper (de Blok et al. 2001) radial density profiles as generated by Hα rotation curves are presented for a number of LSB systems. In at least five out of $\sim$ 40 cases the profiles cannot be reconciled with NFW halos.

Comparing the normal galaxies to the LSB systems in the Ursa Major cluster, Tully & Verheijen (1997) conclude that certainly the LSB galaxies must be sub maximal. The

NGC 3992 group is part of the Ursa Major cluster and the three companions of NGC 3992 are small LSB galaxies. Consequently, observations and analysis of the rotation curves of these companions is of interest. Not only is it important to make a comparison with the other galaxies in the cluster, but the derived rotation curves may also shed extra light on the universality of CDM generated mass structures.

The NGC 3992 group consists of the large barred spiral galaxy NGC 3992 and its three small companion galaxies UGC 6923, UGC 6940, and UGC 6969. The group had already been observed in H I by Gottesman et al. (1984) and later by Verheijen (1997) and by Verheijen & Sancisi (2001). Both these observations suffer from a limited resolution or limited S/N level. In order to derive a detailed rotation curve of a large barred spiral, NGC 3992 was observed again with the Westerbork Synthesis Radio Telescope. The results and analysis of these observations are presented by Bottema & Verheijen (2002, hereafter Paper I). Within the same field there are the H I structures of the companions. Because the total amount of material appeared to be quite comprehensive and because the subjects of barred and dwarf galaxies are relatively unrelated, it was decided to present matters in two papers. A detailed description of the observations and data handling has already been given in Paper I; here only the observing parameters are summarized in Table 1.

For the UMa cluster a Tully-Fisher relation (Tully & Fisher 1977) has been constructed by Verheijen (1997), which shows two anomalies for the NGC 3992 group. Firstly, the massive galaxy NGC 3992 is too faint for its maximum rotation. Related to this, the derived mass-to-light ratio of that galaxy is nearly a factor two larger than that of other spirals. Secondly, the two companions UGC 6923 and UGC 6969 have the same maximum rotation yet differ by a factor of five in total luminosity. That represents a clear source of scatter in the Tully-Fisher relation. To investigate these matters, luminosities, colours, and M/L ratios of the group members will be compared in the present paper. For convenience a listing of the main parameters of the galaxies is given in Table 2.

The distance to the UMa cluster as a whole and to NGC 3992 in particular has not yet been determined precisely. Sakai et al. (2000) give a distance of 20.7 ± 3.2 Mpc following from a Tully-Fisher analysis using the cepheid distances to local galaxies. On the other hand, for a similar analysis, Tully & Pierce (2000) derive a distance to the UMa cluster of 18.6 Mpc, probably with the same error as that of Sakai et al. In a recent re-evaluation of the HST distance scale project (Freedman et al. 2001) the distances to the local calibrator galaxies have decreased by $\sim 5\%$ and consequently the distances to UMa of 20.7 and 18.6 Mpc should also be decreased by that amount. As for now, a distance of 18.6 Mpc seems reasonable and has been adopted in the present paper. This distance differs, however, from the 15.5 Mpc used in earlier studies of the UMa cluster by Tully et al. (1996) and by Verheijen (1997).

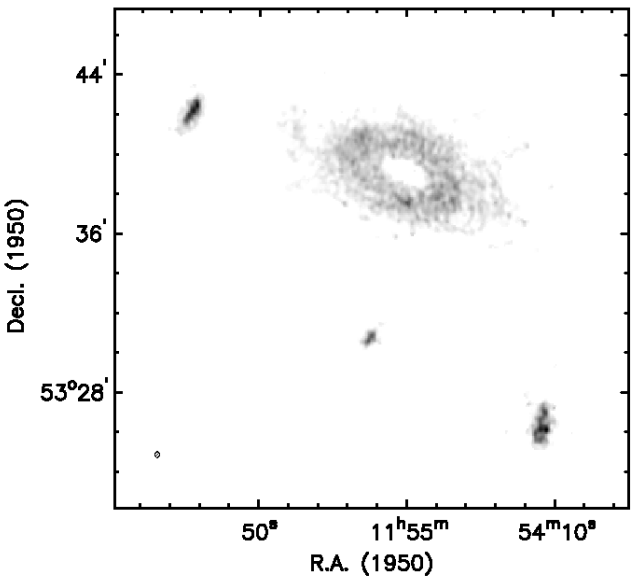

Fig. 1. Greyscale image showing the full resolution total H I map of NGC 3992 and its surroundings. From top left to bottom right the three companions, UGC 6969, 6940, and 6923 are clearly visible; their H I column densities are larger than that of the main galaxy. Note the central H I hole of NGC 3992, at the region of the bar. The beam is indicated in the lower left, the greyscale is linear from 0.2 10^{20} to 34.8 10^{20} H-atoms cm^{-2}.

2. Total H I

To have an overview of the H I distribution in the group, the total H I map at full resolution is displayed in Fig. 1. Immediately obvious is the central hole in the gas distribution of NGC 3992 at exactly the position of the bar. Furthermore, NGC 3992 has a faint gas extension outside its stellar disc. This is contrary to the companions where the H I distribution ends abruptly at the optical edge of the galaxy. A possible explanation for this is stripping of the gas from the companions when these have passed by, or interacted with NGC 3992. For the companions no effort has been made to construct an H I distribution at lower resolution. That would in practice mainly result in a smearing of the gas somewhat over the edge, thereby dominating the additional gas that might be there. Moreover, when determining the gas kinematics for the companions the additional sensitivity at lower resolution does not outweigh the benefits of the higher resolution.

The position and amount of H I gas has been determined the same way as for the main galaxy; using the conditional transfer method for the full resolution data. For all galaxies the same smoothing and filtering parameters have been used (see Paper I). Addition of the signal in

each channel map at the position of the galaxies gives the H I profiles. These were already displayed in Fig. 4 of Paper I, together with that of NGC 3992. All the signal of the companions falls within the H I profile of the main galaxy. Integration of the data cube along the velocity direction results in the total H I maps. These are displayed on the optical image in Figs. 2, 3, and 4 for respectively UGC 6923, 6940, and 6969. For the three galaxies the neutral hydrogen gas generally coincides with the optical galaxies; there are no large displacements or attached filaments. In the case of UGC 6923 (Fig. 2) a slight correspondence of the gas with optical arms is visible. For UGC 6969 (Fig. 4) there is somewhat more gas on the North West side compared to the South East side. The small protrusion on the South East side has a velocity deviating by 40 km s^{-1} from the general velocity field. It has approximately a radial velocity halfway between the value of the general field and the systemic velocity (see Fig. 9, top panel). It might be a gas cloud accreting on the galaxy or in the process of being tidally stripped. Anyway, it has not been taken into account for the determination of the rotation curve. The smallest galaxy (UGC 6940) is so moderately resolved that not much can be said about the H I gas in relation to the optical, except that in general both coincide.

Integration over velocity and space gives the total H I flux, which amounts to 7.82, 1.92, and 5.43 Jy km s^{-1} for respectively UGC 6923, 6940, and 6969. For a distance of 18.6 Mpc this translates in total H I masses of respectively 6.38 10^8, 1.57 10^8, and 4.44 10^8 $M_\odot$.

The surface density as a function of radius has been constructed the same way as for the main galaxy. Elliptical annuli with orientations given by the rotation curve fit were projected on the surface brightness map. The emission was averaged over these annuli and scaled such that integration of the radial profile gives the same total H I mass as found above. The resulting radial density profile is shown in Fig. 5 for all three companions. For UGC 6923 and UGC 6969 there is only a small amount of beam smearing and the derived radial density profile is a good representation of the actual gas distribution. This is not valid for UGC 6940; in that case the profile given in Fig. 5 may deviate somewhat from the true radial distribution.

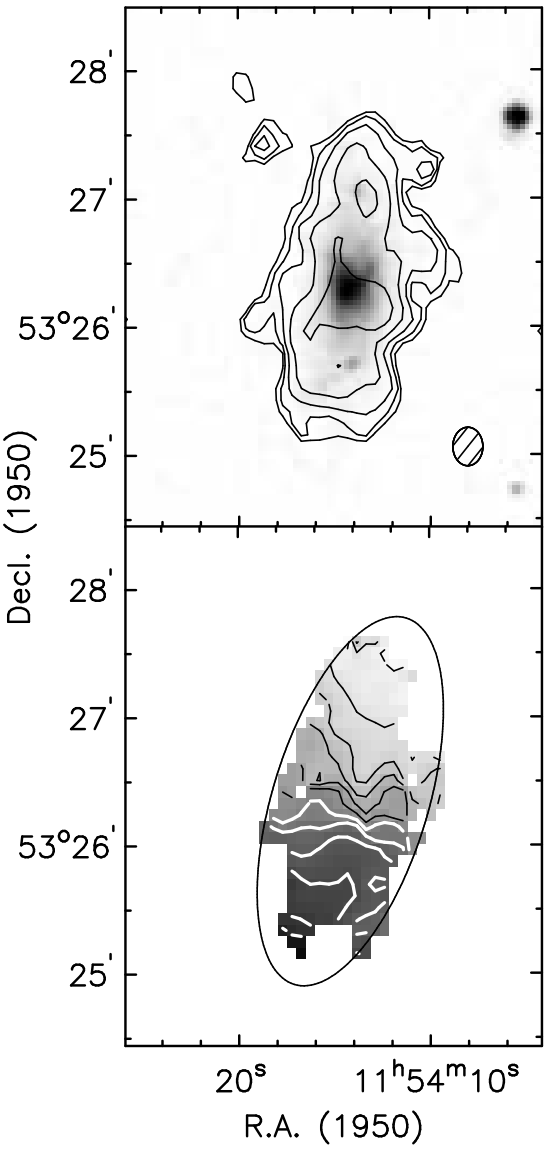

Fig. 2. *Top:* Full resolution total H I map of UGC 6923 superposed on the optical image. Contour levels increase by a factor of two from 1.39 10^{20} to 44.3 10^{20} H-atoms cm^{-2}. *Bottom:* Full resolution velocity field of UGC 6923. The first black contour next to the white contours is at the systemic velocity of 1066 km s^{-1}. Contours differ by 15 km s^{-1} and increase from bottom to top. The ellipse indicates the position of the outermost tilted ring for which a rotational value has been determined.

3. Construction of the velocity fields

Inspection of the line profiles revealed that at certain positions in the galaxy UGC 6923, these are rather skewed. This skewness must be ascribed to beam smearing. If in one beam there is a gradient in the true velocity field, extensions will be created in the observed line profiles towards the systemic velocity. It is difficult, if not impossible to analytically correct for such beam smearing (see Begeman 1989). A good approximation of the true radial velocity, however, is that velocity at exactly the peak of the asymmetric profile. Of course, this is only valid if the velocity field, gas distribution, and resulting line profiles are regular. The problem is now to find this true peak position.

In the past attempts have been made to do so by, for instance, correcting the velocity side furthest from systemic for the instrumental resolution and intrinsic dispersion (Sancisi & Allen 1978). That method is rather dependent on the experience of the interpretator and not generally applicable. Another method is fitting a double

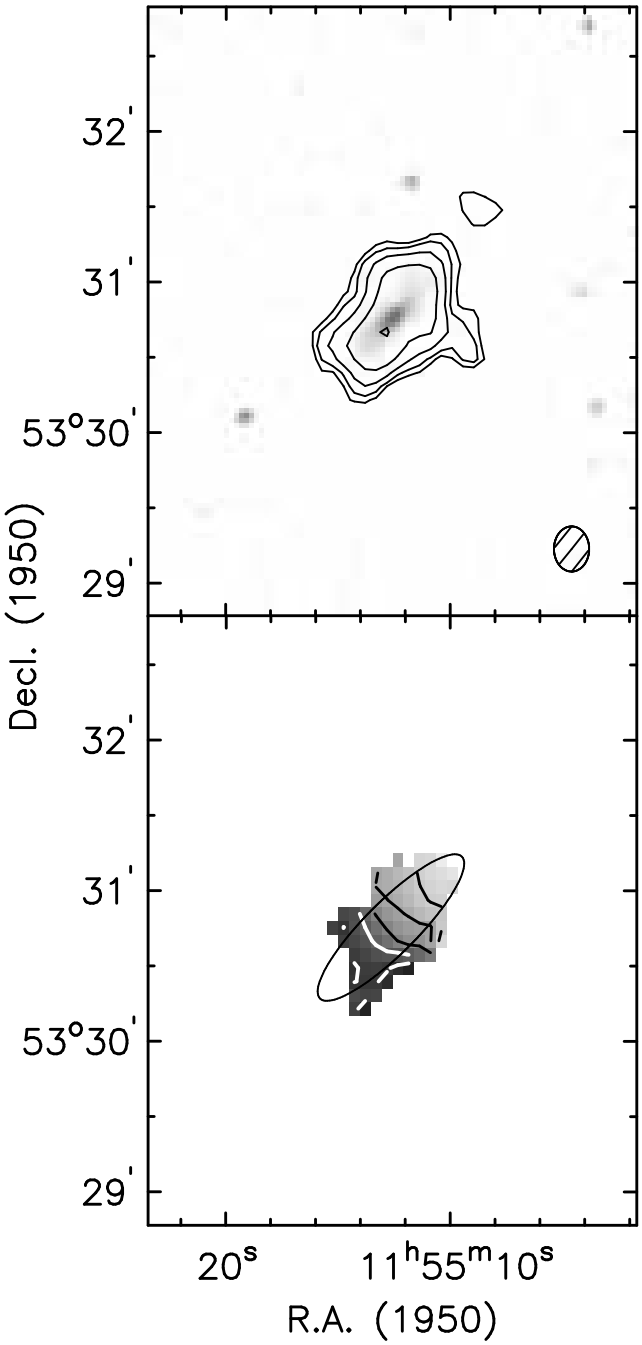

Fig. 3. As for Fig. 2, but now for UGC 6940 having a systemic velocity of 1107 km s^{-1}.

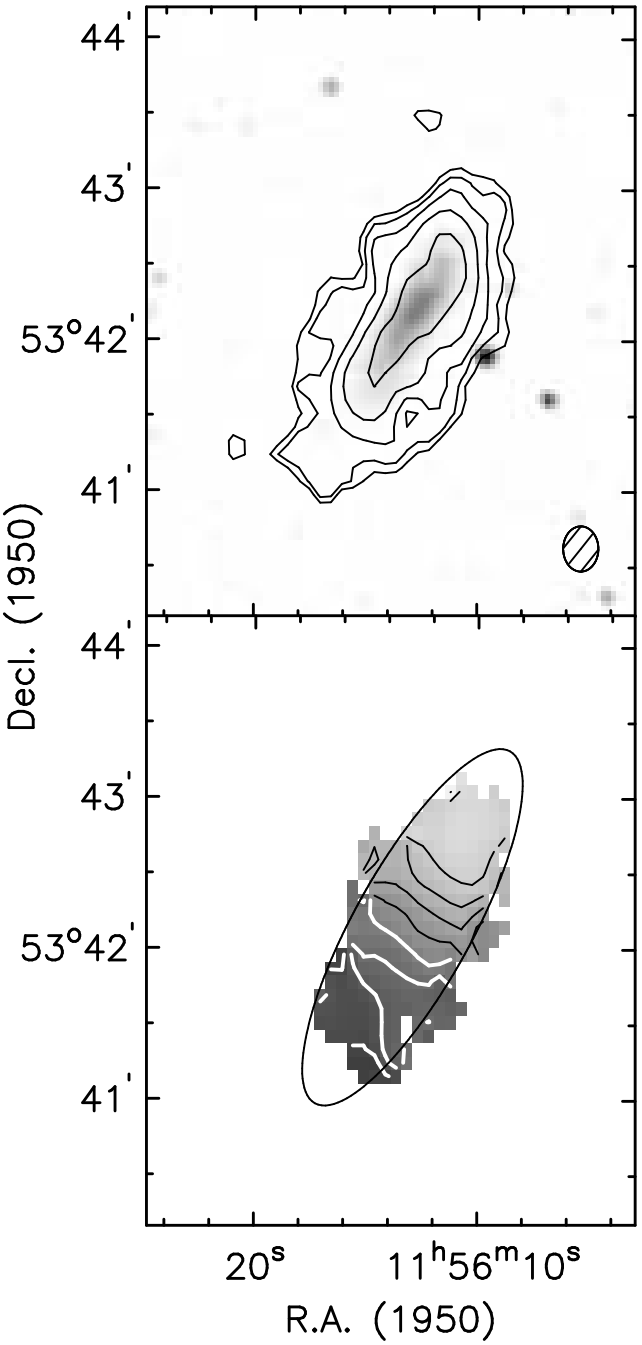

Fig. 4. As for Fig. 2, but now for UGC 6969 having a systemic velocity of 1114 km s^{-1}.

Gaussian to the line profile and retaining only the one furthest from the systemic velocity. The main problem associated with this method is that observed profiles are rarely sampled by more than four to five data points, while two Gaussians already have six free parameters. Resulting fits may therefore be unphysical. Rather one would like to fit a skewed analytical profile to the data with only four free parameters. A suitable function is a Gauss-Hermite polynomial expanded so as to include only one asymmetric ($h3$) term (van der Marel & Franx 1993):

$$f(v) = a e^{\frac{-(v-b)^2}{2c^2}} \left\{ 1 + h3 \left[1.1547 \left(\frac{v-b}{c} \right)^3 - 1.1732 \left(\frac{v-b}{c} \right) \right] \right\}, \quad (1)$$

where v is the radial velocity and a, b, c, and $h3$ are the parameters to be determined. In general a, b, and c de-

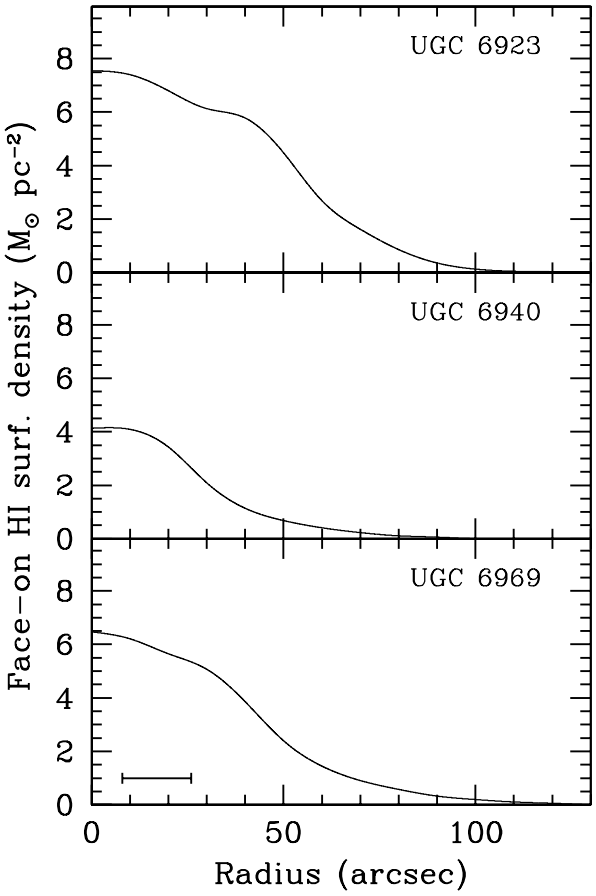

Fig. 5. Deprojected H I surface density as a function of radius for the three companions. The surface densities were obtained by averaging the total H I maps over elliptic annuli with the same orientations as used for the rotation curve determination. The approximate FWHM resolution is indicated by the errorbar.

viate slightly from the Gaussian fit parameters if a pure Gaussian had been fitted to the data. The true maximum of the profile is not at a velocity equal to the value of b, but can easily be found numerically for every case.

The steps in determining the velocity field are in principle the same as those followed for the main galaxy. The initial estimates for the fit were found by fitting a Gaussian to the conditionally transferred data cube. With these estimates the skewed profile given above was then fitted to the whole (full resolution) data cube. Line profiles with dispersions less than 10 km s^{-1} and amplitudes less than 1.5 times the noise level were rejected. The position of the maximum was then adopted as the value for the velocity field. The field was inspected for continuity which led for all galaxies to the removal of typically less than 10 pixels. Resulting velocity fields are displayed in the bottom panels of Figs. 2, 3, and 4 for UGC 6923, UGC 6940, and UGC 6969 respectively. The velocity field of UGC 6923 shows an amount of differential rotation while the other two galaxies have a velocity morphology which is close to solid body. As mentioned before, the South East extension of UGC 6969 has a deviating velocity. Such a deviation should not be included in a rotation curve fit to the velocity field an has therefore been removed from the velocity field of UGC 6969 in Fig. 4. It is, however, still present in the major axis x,v diagram in Fig. 9, top panel. Except for this feature there are no appreciable irregularities present in the velocity fields.

As a bonus also the $h3$ image for the galaxies is generated. For UGC 6923, the galaxy for which this asymmetric fitting was devised, the $h3$ field is symmetric with respect to the centre. Values of $h3$ are positive on one side along the major axis and negative on the other side of the centre. This is a clear signature of beam smearing. The other galaxies only show a very small and peculiar asymmetry which will be discussed in the next section. The specific beam smearing figure is not present.

4. The rotation curves

A tilted ring model has been fitted to the velocity fields of the companion galaxies to obtain the rotation curves. Non overlapping rings have been used with a width of $10''$ and a weighting factor has been assigned to the data proportional to the cosine of the angle measured from the major axis. In first instance the dynamic position has been determined using an initial estimate of the rotation velocity and orientation angles. Having this centre fixed, first the position angle was determined, then the inclination, and after fixing that, the rotation curve.

The application of this procedure to the three companions is not straightforward, which is caused by the close to solid body nature of the velocity field. If one has the hypothetical case of a pure solid body then the velocity contours are all straight lines perpendicular to the major axis. By means of a tilted ring fit it is then not possible to determine independently the dynamical position nor is it possible to obtain the inclination. In such a case it has to be assumed that the optical position and inclination coincide with the kinematic position and inclination. For H I gas within the optical region of a galaxy this is generally a valid assumption. The three companions have velocity fields with an appreciable solid body content. Therefore in some cases for some parameters optical values have to be used, which will be a reasonable approximation because the gas does not extend outside the optical image. For the outer tilted rings there will be positions along the rings with no determined H I radial velocities. To illustrate this, the outermost ring for which a rotational value has been determined is displayed as an ellipse on top of the velocity fields. In that way it can be inspected which positions of the galaxy are, and which are not, contributing to the rotation curve determination.

The least squares fitting method gives errors, but these are only formal errors, which are not always a good rep-

resentation of the true deviation from the data. To come up with a more realistic error of the rotational velocity, the fitting procedure has been repeated for the receding and approaching side of the galaxy separately. Positions and orientation angles were kept fixed at the same values as for the whole galaxy and rotation velocities were determined. The difference in rotation of the two sides gives a better representation of the true error. The final error is then given by the quadratic sum of the formal fit error plus half the difference between the two sides.

The rotation curve fitting procedure will now be discussed for the three companions separately:

4.1. UGC 6923

There was no drifting of the dynamic centre as a function of radius, which can therefore be determined quite accurately. The systemic velocity is 1066 ± 2 km s^{-1} and other fitted parameters can be found in Table 3. Further steps in the fitting procedure are illustrated in Fig. 6. In the top panel the position angle is shown when all three parameters, rotation, inclination and pa were left free. The position angle does not show a trend as a function of radius and was fixed at a constant value of 343°. The middle panel of Fig. 6 gives the fit result for the inclination after the pa is fixed.

As noted above, it is difficult to get well determined, independent kinematic inclination values. The optical inclination for UGC 6923 is 66° for an adopted q_0 of 0.11. This inclination is given by the dashed line in Fig. 6 (middle panel), and is not inconsistent with the kinematic inclination. Around a radius of 40″ the kinematics prefers a somewhat smaller inclination which is likely caused by the enhanced H I density and accompanying slightly deviating velocity field West of the centre. I feel confident that the constant optical inclination is a good representation of the actual gas kinematics.

The lower panel shows the final rotation curve for that fixed inclination. Errors superposed on the points are already those when the difference between the two sides has been taken into account. All numerical values for the rotation curve of UGC 6923 are given in Table 3. The outermost ring for which the rotation is determined has a radius of 90″ and is displayed as an ellipse in Fig. 2, bottom panel. This ring still picks up a number of radial velocity points at diverse and independent positions of the galaxy. Therefore the rotational value at that radius is a reliable and significant measurement.

4.2. UGC 6940

The velocity field of UGC 6940 is close to solid body and so small compared to the beam that it was impossible to determine independently the dynamical centre. Therefore it had to be assumed that the spatial position of the optical nucleus coincides with the galaxy's dynamical centre.

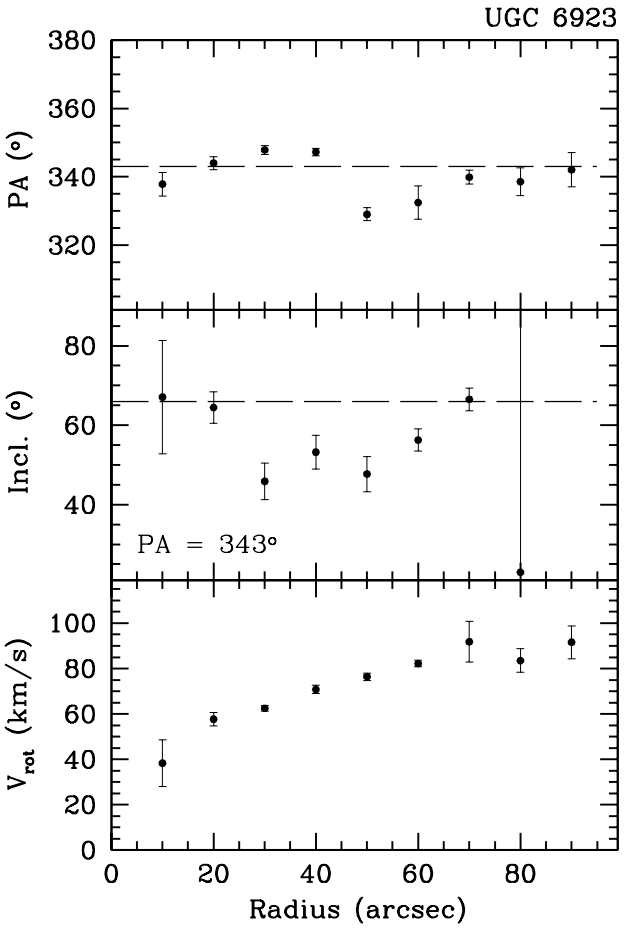

Fig. 6. Determination of the rotation curve by a tilted ring fit for UGC 6923. In first instance the orientation angles and rotation velocity were all left as free parameters producing position angles as a function of radius (top panel). The PAs were fixed at 343° indicated by the dashed line, and the fitting procedure was rerun producing the inclinations (middle panel). The optical value of 66° was used for all inclinations (dashed line). In the bottom panel the final rotation curve is presented.

Using that position and a guess for the rotation and orientation angles it was possible to get a solid value for the systemic velocity of 1107 ± 2 km s^{-1}. All fit values for this galaxy are summarized in Table 4. Next steps in the fitting procedure are illustrated in Fig. 7, analogous to, but slightly different from Fig. 6. The middle panel shows the fit for a free rotation, pa, and inclination, while the top panel gives the fit for the position angle with the inclination fixed at the optical value. The adopted constant values for the position angle and inclination are equal to the optical values and nicely compatible with the results of the tilted ring fit, as can be seen by the dashed lines in Fig. 7. The rotation curve plus the final errors are presented in the lower panel.

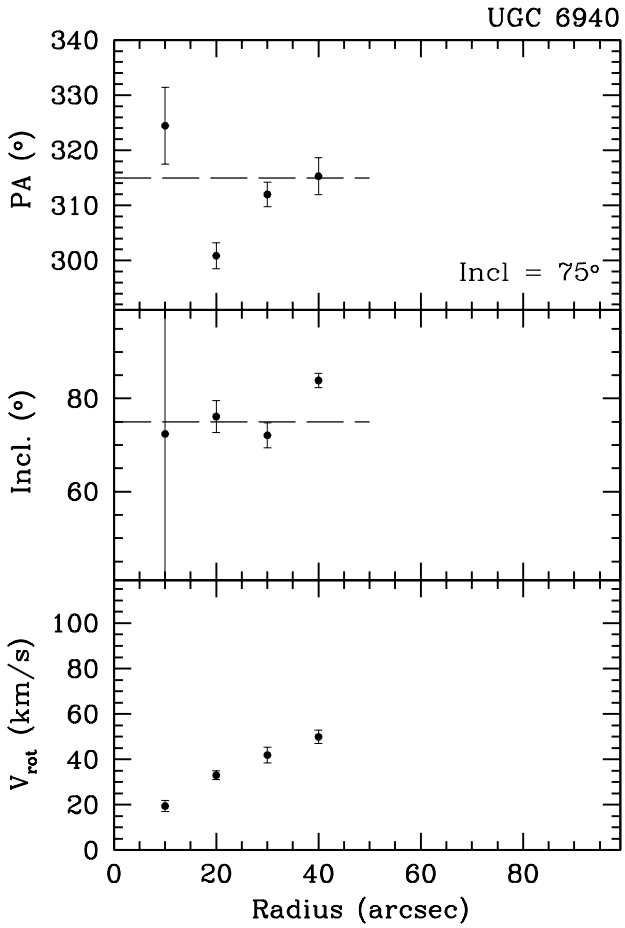

Fig. 7. As Fig. 6, but now for UGC 6940. For this galaxy the optical values for both, the position angle and inclination had to be adopted, being consistent with the data points in top and middle panel.

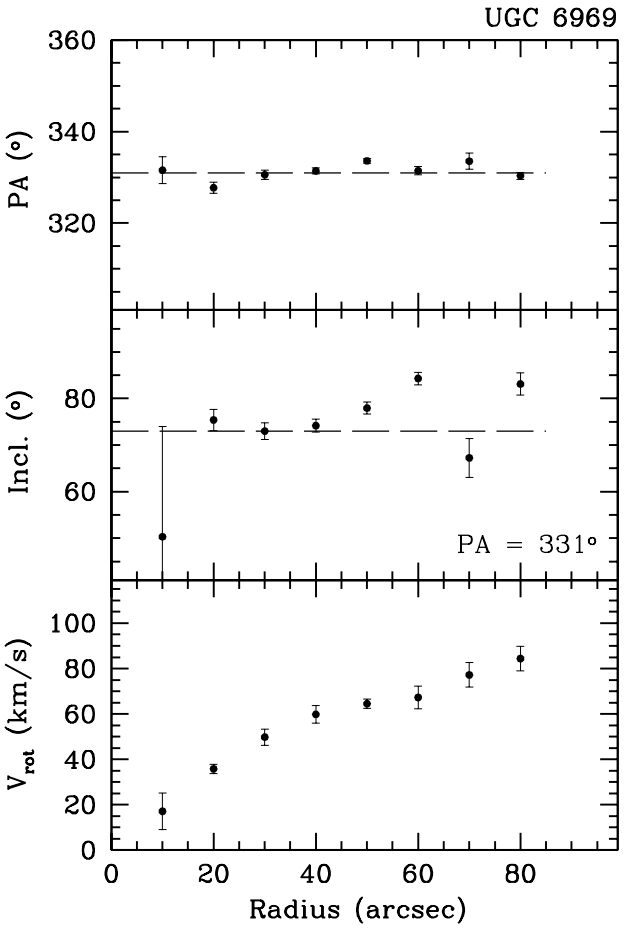

Fig. 8. As Fig. 6, but now for UGC 6969.

4.3. UGC 6969

Using an initial estimate of the rotation together with fixed values of the orientation angles resulted in a slight drift of the centre as a function of radius of 20″ in the spatial direction and 10 km s^{-1} in velocity, over the 80″ radial extent of the tilted ring fit. To assess the reality of the drift, in a first iteration the dynamical centre was fixed at the radially averaged value, and a fit of the rotation was made. This rotation curve was used as a next guess to redetermine the centre. Now the drift had disappeared and the constant value of the dynamical centre is given in Table 5. The optical centre was measured and was only 3″ away from the dynamical centre position, which is well within the measurement errors. This demonstrates that the iteration has converged to a reliable value, though for the nearly solid body velocity field of UGC 6969 the procedure can never be done in a completely independent manner. Having the centre fixed, the further fitting process is illustrated in Fig. 8. There is no trend as a function of radius for the fit of the orientation angles. Again the optical values (for $q_0 = 0.11$) are fully compatible with the results of the tilted ring fit, and were adopted. The rotation curve with its proper errors is shown in the lower panel of Fig. 8.

4.4. Discussion

To show the reliability and consistency of the method to derive the rotation curves, in Fig. 9, the determined rotational velocities have been converted to radial velocities and plotted on the x,v diagrams along the major axis. For all three galaxies the rotation points are at the positions where one would expect them to be. NGC 6923, for example, shows the skewed profiles in Fig. 9. The rotation curve of this galaxy nicely follows the positions of maximum intensities of the x,v diagram, demonstrating that the skew linefit procedure is correct.

In some cases, at the outer positions of the gas distributions there is a rotational point given while there is no gas associated with it in the x,v diagram. This is caused by the fact that the gas is spatially not distributed in an

elliptical shape similar to the orientation of the kinematic tilted rings. Gas may then not be present along the major axis, while there is still gas with associated radial velocities at other positions along the tilted ring. For instance for UGC 6969 at the NW side of the galaxy, at that spot there is no H I gas. Still the outermost data point of the rotation curve is determined from radial velocities of 22 pixels. Note that for this galaxy the cloud with deviating velocity is displayed on the SE perimeter of the x,v diagram. The affected region is not included in the tilted ring fit, but still the rotation curve is fully consistent with the x,v diagram in the sense that it correctly traces the envelope of the gas distribution (Sancisi & Allen 1978).

Though UGC 6923 and UGC 6969 have nearly the same maximum rotation the shapes of the rotation curves are different. UGC 6969 has a rotation curve which has more a solid body signature. Is this real? Inspection of the x,v diagrams in Fig. 9 demonstrates that these diagrams are indeed rather different for both galaxies. UGC 6923 shows signs of beam smearing which can be observed in case of differential rotation. UGC 6969, on the other hand, does not show these signs and cannot show these signs if the galaxy has a rotation close to solid body. In order for a differentially rotating galaxy to show a solid body x,v diagram, the gas must have a central density depression in combination with substantial beam smearing. As can be seen in Fig. 5, where the observed radial density profile is given, this is not the case. We must therefore conclude that the different shapes of the two rotation curves is indeed real.

For the three companions Verheijen has also derived the rotational parameters. His resolution is much worse, however, and he was forced to use optical orientation values from the onset. This study confirms that these optical values are appropriate and hence the global rotation of Verheijen is equal to the present rotation. With the higher resolution and better signal to noise it is now possible to derive rotation curves with more details and going somewhat further out.

Looking at Fig. 9, one can at first notice that all companions rotate in the same way with respect to the plane of the sky. Secondly, both UGC 6969 and UGC 6940 exhibit a slight skewness of the line profiles in the sense that the tail extends to higher velocities. This is visible along the whole major axis and does not change significantly with position. A possible explanation might be that we are witnessing the effect of tidal forces when the two companions move past the large galaxy NGC 3992.

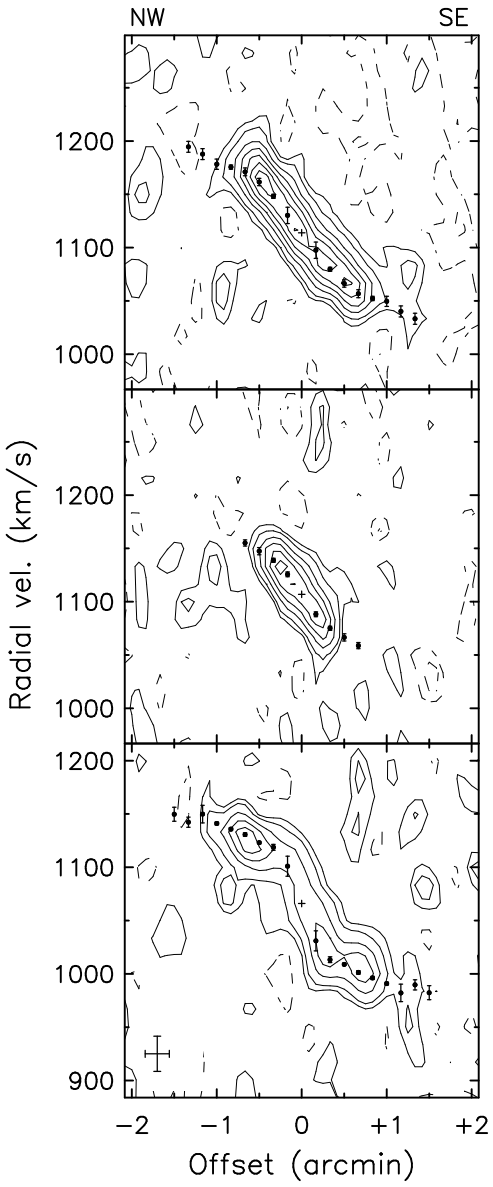

Fig. 9. The rotation curves of the companions converted to radial velocities, overplotted on a full resolution position - velocity map along the major axes. Top, middle, and bottom panels are for UGC 6969, UGC 6940, and UGC 6923 respectively. The cross indicates the position of the dynamic centre; contour levels are at -3.92 and -1.96 K (dashed), and at 1.96, 3.92, 7.84, 11.8, 15.7, 19.6, and 23.5 K. One can notice that for UGC 6923 (bottom panel) a satisfactory correction for skewed line profiles has been made.

5. Decomposition of the rotation curves

The decompositions of the rotation curves have, in principle, been done in the same way as for the major galaxy. The I-band photometry of Tully et al. (1996) was used to represent the radial mass profile of the galaxies (see Fig. 10). Locally isothermal stellar discs were assumed with a z_0 value of one fifth of the scalelength. For the gas the radial distribution was taken equal to that given in Fig. 5, multiplied with a factor of 1.4 to account for Helium, while the disc was infinitely thin. Two kinds of dark halo have been considered, a pseudo isothermal one and an NFW halo.

The density distribution $\rho_{\rm h}$of a pseudo isothermal halo is given by

$$\rho_{\rm h} = \rho_{\rm h}^0 \left[1 + \frac{R^2}{R_{\rm core}^2}\right]^{-1}, \quad (2)$$

with a rotation law

$$v_{\rm h} = v_{\rm h}^{\rm max}\sqrt{1 - \frac{R_{\rm core}}{R}\arctan\left(\frac{R}{R_{\rm core}}\right)}, \quad (3)$$

where $R_{\rm core}$ is the core radius related to the maximum rotation of the halo $v_{\rm h}^{\rm max}$ by

$$v_{\rm h}^{\rm max} = \sqrt{4\pi G\rho_{\rm h}^0 R_{\rm core}^2}. \quad (4)$$

For an NFW halo the density distribution takes the form

$$\rho_{\rm NFW} = \frac{\rho_i}{(R/R_s)(1+R/R_s)^2}, \quad (5)$$

where R_s is a characteristic radius and ρ_i is related to the density of the universe at the time of collapse. The rotation curve $v_{\rm NFW}$ following from this distribution is

$$v_{\rm NFW} = 2.15\, v_{\rm max}\sqrt{\frac{R_s}{R}\ln\left(\frac{R}{R_s}+1\right) - \frac{R_s}{R+R_s}}, \quad (6)$$

where the maximum rotation $v_{\rm max}$ is reached at a radius of 2.16 R_s. When a certain cosmology is chosen the structural parameter becomes related to the total mass of the halo. In this case, there is a relation between the characteristic radius R_s and the maximum rotation. Presently I assume the current concordance model for the cosmology: a low density CDM universe with a flat geometry, called CDMΛ with $\Omega_0 = 0.25$, $\Lambda = 0.75$, and a Hubble constant of 75 km s^{-1} per Megaparsec. For that cosmology Navarro et al. (1997) relate the parameter M_{200} to $v_{\rm max}$ in their Fig. 7. Some manipulation with equations leads to the following relation between R_s and $v_{\rm max}$

$$\frac{R_s}{[\rm kpc]} = 0.0127\left(\frac{v_{\rm max}}{[\rm km/s]}\right)^{1.37}, \quad (7)$$

such that when Eqs. (6) and (7) are combined there is only one free parameter left for the dark halo.

Besides the specific NFW profile, cosmological CDM simulations also generate a certain scatter in these profiles. Bullock et al. (2001) give in their Fig. 4 the scatter of the concentration parameter c, which appears to be independent of the halo mass. The positive 1σ deviation is approximately 0.105 on a ^{10}log scale (factor 1.27) but the negative 1σ deviation from the concentration parameter appears to be larger, approximately 0.21 in ^{10}log equal to a factor 1.62. A different investigation by Jing (2000) gives for a ΛCDM cosmology and for the most virialized halos a 1σ scatter of 0.17 on a natural log (ln) scale (factor 1.19). For less virialized halos the scatter is a factor 1.28 and on average it is 1.22. All these numbers differ somewhat, but a factor 1.28 or a 1σ deviation in $\Delta\ln c$ of 0.25 seems a reasonable compromise. Equation (7) has been derived from the M_{200} versus $v_{\rm max}$ relation and it is easy to demonstrate that a scatter in $\ln(c)$ then translates in exactly the same scatter in $\ln(R_s)$. For a 3σ less concentrated dark halo, the coefficient in Eq. (7) has to be multiplied by a factor $e^{3\times0.25}$, increasing it to 0.027. Such a 3σ deviation is considered as a limit to the NFW functionality.

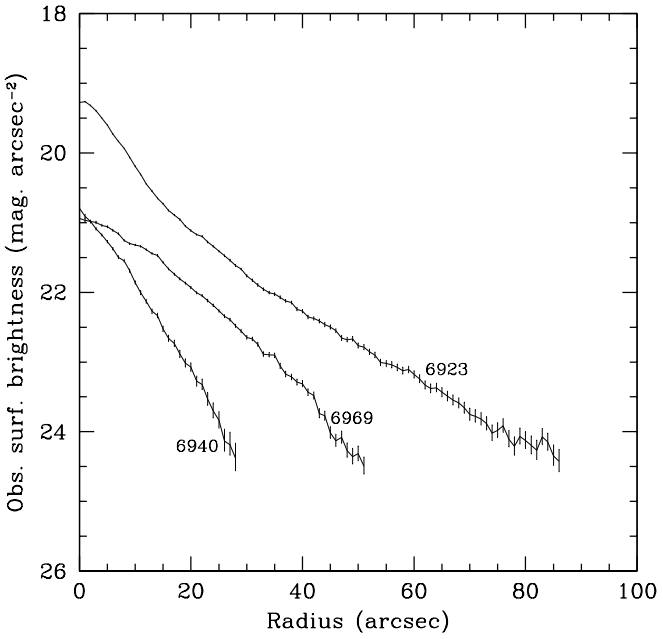

Fig. 10. Radial profiles in the I-band for the three companions as measured by Tully et al. (1996).

The results of the rotation curve decompositions are shown graphically in Figs. 11, 12, and 13 for respectively UGC 6923, 6940, and 6969, while Table 6 gives the numerical values. For an isothermal halo three cases have been investigated. A maximum disc situation where the contribution of the stellar disc to the total rotation is maximized, shown in the top panel of Figs. 11 to 13. Also a minimum disc case is investigated, where there is simply no stellar disc at all, of which the results are only given in Table 6. Lastly, the decomposition is given for $(M/L)_I = 0.82$ in the middle panels of the Figs. 11 and 13 and in the lower panel of Fig. 12. This situation corresponds to the 63% criterion for large galaxies and the ensuing M/L ratio. A derivation of this mass-to-light ratio of 0.82 in the I-band is given in Sect. 6.

In case of maximum disc the M/L_I ratio of the dwarf galaxies ranges between 1.6 and 1.8 while the core radius is comparable to or larger than the outer measured radius of the gas. Reducing the stellar disc contribution results in a smaller core radius of a few kpc. In all three cases the fits to the observed data points are equally good and so, as usual, from a rotation curve decomposition nothing can be deduced about the contribution of the stellar disc. If, on the other hand, one assumes $(M/L)_I = 0.82$ for all three galaxies and one compares the determined dark halo rotations in Fig. 14 one notices that the dark halos of the three companion galaxies are nearly equal. This is striking because the total luminosities of the galaxies cover a range of a factor 16. Do we have a situation where there are three identical dark halos with different luminous galaxies embedded?

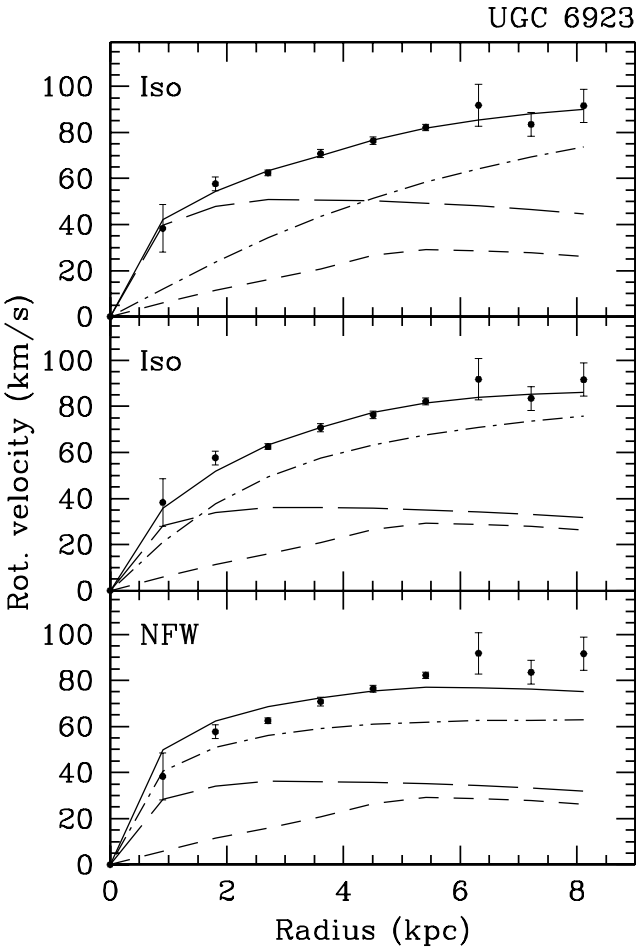

Fig. 11. Rotation curve decompositions for UGC 6923. The dots are the observed rotational data and the full drawn line is the fit to these. Individual contributions of the disc (long dashed line), gas (short dashed line), and dark halo (dash - dot line) are indicated. Numerical values are given in Table 6. *Top:* An isothermal halo maximum disc fit. *Middle:* A decomposition for an isothermal halo and $(M/L)^I_{\rm disc} = 0.82$. *Bottom:* For an NFW-CDMΛ halo with $(M/L)^I_{\rm disc} = 0.82$.

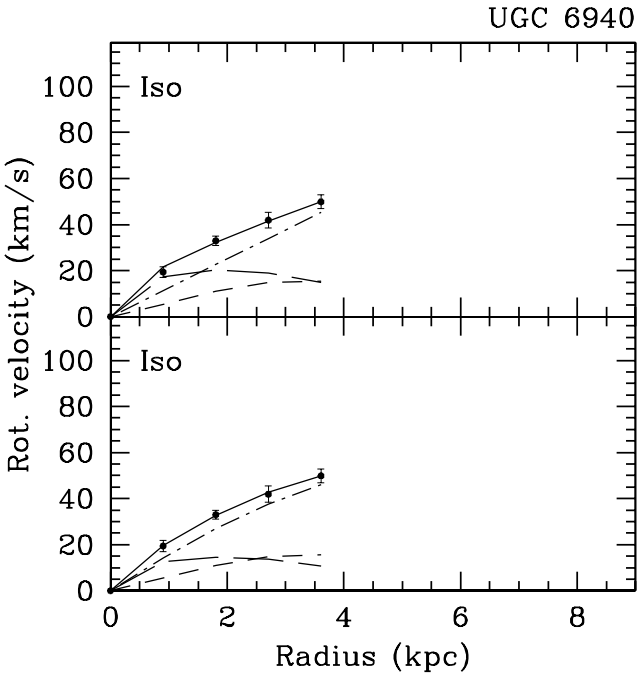

Fig. 12. As Fig. 11, but now for UGC 6940. In this case no NFW fit has been made.

Let us leave out UGC 6940 because the halo rotation is not established very far out. UGC 6923 and UGC 6969 differ by a factor five in luminosity, while having approximately the same dark halo rotation. The effect of this can be seen nicely in Figs. 11 and 13, middle panels. UGC 6969 has the solid body rotation and the dark halo dominates over the whole radial extent. UGC 6923 is more differentially rotating which is caused by the larger disc mass contribution simply because the disc of UGC 6923 is more massive. For a $(M/L)_I$ of 0.82 the stellar disc still dominates the rotation for radii less than 1.5 kpc. The differences between these two galaxies have an interesting effect on their positions in the Tully-Fisher relation, which will be discussed in the next section.

NFW decompositions have been made for UGC 6923 and UGC 6969 of which the results in case of a fixed $(M/L)_I = 0.82$ are presented in Figs. 11 and 13, lower panels. For UGC 6923 the fit of the strict NFW functionality (Eqs. 6+7) is slightly off in the inner and outer parts. If the M/L ratio is reduced to 0.0 or when a moderate deviation from the strict profile within statistical limits is allowed, a good agreement between fit and data points can be achieved. Consequently for UGC 6923 both the isothermal and NFW halo can give a good description of the rotation.

For UGC 6969, however, the situation is different. As can be seen in Fig. 13, the strict NFW halo cannot fit the observations. A 3σ less concentrated halo has an R_s parameter of 8.4 kpc, which is nearly three times as large as for the strict case. Even then the fit is not good; the inner and outer rotational points deviate too much from the total fitted rotation curve. Decreasing the M/L ratio of the disc barely improves matters because the disc contribution is already small. If the R_s and $v_{\rm max}$ parameters are left unrelated to each other, the then ensuing two parameter fit diverges to very large values of R_s and $v_{\rm max}$. In such a case a small galaxy is embedded in an unrealistically large dark halo. As discussed in Sect. 4, the x,v diagram of UGC 6969 in combination with the derived radial density structure shows that there is no apparent beam smearing present. In addition, beam smearing is ex-

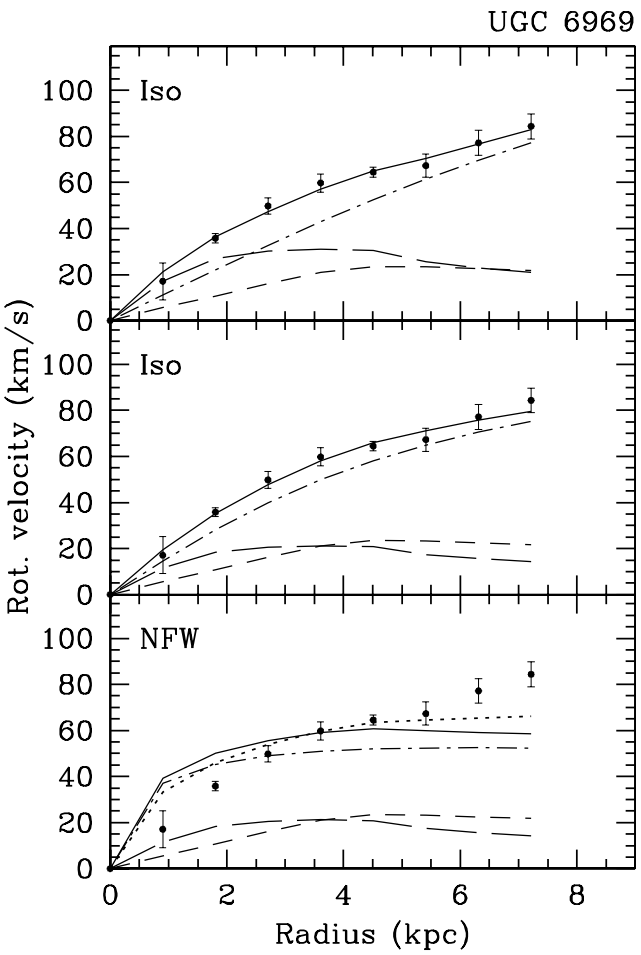

Fig. 13. As Fig. 11, but now for UGC 6969. In addition the dotted line in the lower panel gives the fit of an NFW halo being less concentrated by 3σ from the standard functionality.

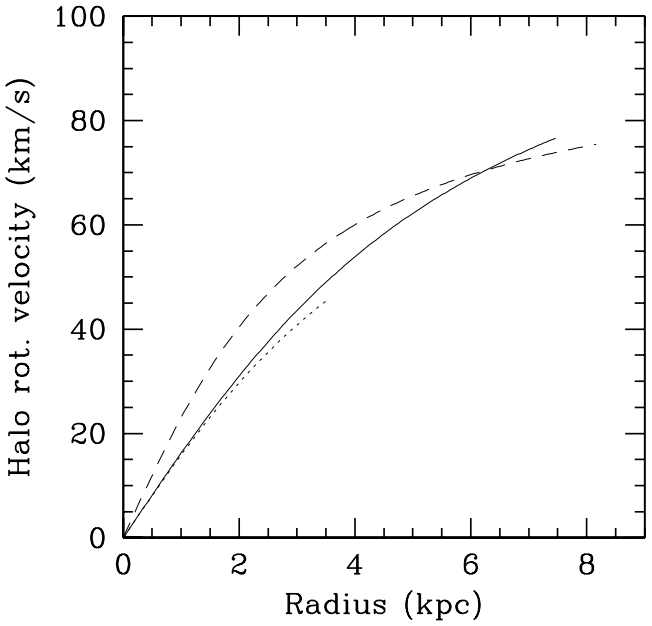

Fig. 14. Rotation curves of the dark halos of UGC 6923 (dashed), UGC 6940 (dotted), and UGC 6969 (full drawn) in case $(M/L)^I_{\rm disc} = 0.82$. Though these galaxies differ by more than a factor of ten in luminosity, their dark halo rotation is identical to within the errors. This suggests that different amounts of luminous matter have settled in identical dark halos.

pected to occur only in the most edge-on or most unresolved galaxies (Swaters et al. 2000; McGaugh et al. 2001) while for the more favourable objects, such as UGC 6969, the derived H I rotation curves generally give a good impression of the actual rotation. The possibility remains of a slight amount of beam smearing, but that can never account for the large discrepancy between observations and NFW halo decomposition.

One might wonder why for the isothermal case nearly equal dark halos produce good fits to all the rotation curves and there are problems with one galaxy for an NFW halo. A solution to this controversy can be found by inspection of Figs. 11 and 13. Like for the isothermal situation also for the NFW case the fitted halo rotation curves are very similar for UGC 6923 and UGC 6969. However, an NFW halo has a cusp producing large rotations in the inner regions which can be allowed for UGC 6923 but not for UGC 6969.

6. Comparing the galaxies of the NGC 3992 group

A detailed description now exists for the four galaxies in the NGC 3992 group, though the main uncertainty which remains is the actual ratio of dark to luminous matter. A comparison will be made with the other galaxies of the UMa cluster which may generate additional information. The TF relation combines in principle the kinematics, governed by dark and luminous matter, with the total light. Consequently this relation and the position in this relation of the four galaxies now studied should give insight into the dark matter content. The I-band TF relation will be considered, because one wants a band as red as possible to minimize dust and population effects, while for the near infrared bands the total luminosities of the galaxies are considered somewhat uncertain. Also the following discussion on mass-to-light ratios will be conducted in the I-band. In first instance one then needs the absorption free total light of the four galaxies.

6.1. Absorption corrections

Various prescriptions exist for converting the observed light of a galaxy into absorption free luminosities. For instance the method of Tully & Fouqué (1985), which does a total conversion, while other methods are gen-

erally restricted to a conversion to face-on luminosities. This method gives an internal absorption correction A_X^i for passband X and inclination i of

$$A_X^i = -2.5\log10\left[f\left(1+\mathrm{e}^{-\tau\mathrm{sec}(i)}\right)+(1-2f)\cdot\left(\frac{1-\mathrm{e}^{-\tau\mathrm{sec}(i)}}{\tau\mathrm{sec}(i)}\right)\right]. \quad (8)$$

For an assumed f parameter of 0.1 and τ values of $\tau_B = 0.81, \tau_R = 0.40, \tau_I = 0.28$, and $\tau_{K'} = 0.035$ one determines a correction for a face on galaxy to absorption free $A_X^{i=0}$ of 0.40, 0.21, 0.15, and 0.02 for the B, R, I, and K' band respectively.

The conversion to absorption free absolute magnitudes $M_{T,X}^{b,i}$ in band X is given for galaxies of the UMa cluster at a distance of 18.6 Mpc by

$$M_{T,X}^{b,i} = m_T - A_X^b - A_X^i - 31.35\,, \quad (9)$$

where m_T is the observed total brightness and A_X^b is the Galactic absorption correction which is generally very small. Both these numbers can be found in Verheijen (1997). For the galaxies in the NGC 3992 group the observed total light and the internal absorption corrections according to Eq. (8) are given in Table 7.

There is, however, a vast difference in intrinsic luminosity between NGC 3992 and the three surrounding dwarf galaxies. As demonstrated by Tully et al. (1998) and by Giovanelli et al. (1997) there is a large range in absorption corrections for galaxies with a range of intrinsic luminosities. Bright, large galaxies have a large dust absorption while small and certainly the low surface brightness galaxies have generally a small or even negligible dust absorption. Consequently it is unrealistic to use the Tully-Fouqué equation for these four galaxies. Tully et al. (1998) give an internal absorption correction to face-on (A_X^{i-0}, so no total correction) of

$$A_X^{i-0} = \gamma_X \log(\frac{a}{b}), \quad (10)$$

where $\frac{a}{b}$ is the major/minor axis ratio of the galaxy and γ_X a factor dependent on absolute luminosity corrected for galactic, k-correction, and internal absorption $M_X^{b,k,i}$ given in the I-band by

$$\gamma_I = -0.20\,(16.9 + M_I^{b,k,i}). \quad (11)$$

When the appropriate values for the four galaxies are substituted in Eqs. (10) and (11) one has $A_I^{i-0}(3992) = 0.26$ and $A_I^{i-0}(\mathrm{U6923}) = 0.13$, while for the other two galaxies the correction is zero. Now still an internal dust correction for the face-on situation has to be made. It will be clear that the whole procedure for internal absorption correction is rather uncertain. Therefore at present, taking into account the numbers given by Eq. (8) and the numbers given by the luminosity dependent correction to face-on a total correction has been adopted of 0.52 magnitudes for NGC 3992 and a zero correction for the dwarfs.

6.2. Mass-to-light ratios

In his analysis of the mass distribution of the galaxies in the UMa cluster Verheijen (1997) finds that in case of the 63% criterion the average M/L ratio in the K' band of 10 HSB galaxies (excluding NGC 3992) amounts to 0.38 $M_\odot/L_\odot^{K'}$ with a scatter of 20%. For a maximum disc situation the average mass to light ratio of the same 10 galaxies is 0.60, being a factor 1.6 larger. Because in individual cases the calibration of the K' photometry may be somewhat uncertain this M/L ratio in the K' band is converted to the I-band. To that aim for all non-LSB galaxies of Verheijens sample the K-I colour has been determined, corrected for internal absorption according to Eq. (8). The average of this, $< K'-I >^i$, was -1.55 and is used to convert the average mass-to-light ratio in the K' to the I-band. In case of the 63% criterion one then has $\langle M/L_I\rangle^i = 0.82$ and 1.30 for the maximum disc situation. In Paper I a comparison has been made with M/L_I ratios of a sample of galaxies for which an absorption to face-on only has been made. To convert the average $\langle M/L_I\rangle^i$ of the ten UMa cluster galaxies to a face-on correction only the same factor of 1.27 (0.26 mag.) as for NGC 3992 has been adopted. Then for the maximum disc case results a $\langle M/L_I\rangle^{i-0} = 1.65$ with a range from 0.7 to 2.2.

The three companions have a maximum disc $(M/L_I)^i$ value of $1.7 \pm \sim 0.3$ (see Tables 6 and 7). When applying the total absorption correction to NGC 3992, its maximum disc $(M/L_I)^i$ equals 2.91 ± 0.07 which is a factor of 1.7 larger than that of its companions. Is this consistent? To answer this, the colours of the four galaxies have been used to compare the stellar populations of the systems. The $(B-R)^i$ colours were derived from the luminosities given by Tully et al. (1996) and Verheijen (1997). An absorption correction for NGC 3992 was made using Eq. (8) resulting in $(B-R)^i_{\mathrm{N3992}} = 1.21$ while no absorption corrections for the companions were made giving a $(B-R)^i_{\mathrm{comp}}$ ranging between 0.8 and 0.95. Then, according to Table 1 of Bell & de Jong (2001), population synthesis models predict for such a colour difference a difference in $(M/L_I)^i$ of a factor $1.6 \rightarrow 2.0$, being very consistent with the observed value. Consequently the difference in maximum disc M/L values between NGC 3992 and its companions can well be explained by a different stellar population of the galaxies. There is a caveat, however. In the argumentation it is assumed that the bluer colours of the companions are caused solely by population effects, while in reality a likely lower metallicity may contribute as well in making the companions bluer.

For the UMa cluster the $(M/L_I)^i$ maximum disc value is 1.30 with a range of $0.54 \rightarrow 1.71$. A much larger value of $(M/L_I)^i = 2.91$ or 2.60 if a bulge is allowed is found for NGC 3992. Hence the maximum disc mass-to-light ratio of NGC 3992 is 2.2 times (or 2.0 with bulge) as large as for the cluster in which it should reside. This finding is similar as that for the less well determined K' band photometry

where Verheijen (1997) finds a factor of 2.9 difference. It is not possible to explain the M/L difference by population effects. The average $\langle I-K'\rangle^i$ colour of 22 HSB galaxies in the UMa cluster is 1.55 ± 0.14 while the $(I-K')^i$ colour of NGC 3992 is 1.48, being absolutely normal. For the $(B-I)^i$ colour one has $\langle B-I\rangle^i_{\rm UMa} = 1.35 \pm 0.28$ and $(B-I)^i_{\rm N3992} = 1.52$ which is also normal. The difference in mass-to-light ratio thus has to be explained by another mechanism. Let us first investigate what happens in case of the 63% criterion. Then the average $(M/L_I)^i$ for the cluster galaxies is 0.82 with a range of $0.65 \rightarrow 1.06$. For the best fitting rotation curve decomposition the maximum disc velocity is slightly below 63% and has an $(M/L_I)^i = 1.11 \pm 0.12$. Here the discrepancy between NGC 3992 and the rest of the cluster is less; there is only a factor of 1.35 difference. However when the disc $(M/L_I)^i$ of NGC 3992 is put at the average cluster value of 0.82 the then following disc mass of $54.3\ 10^9$ $M_\odot$ cannot give a reasonable rotation curve decomposition any more. In order to make equal M/L ratios one might consider to put the $(M/L_I)^i$ for NGC 3992 at 1.30 equal to the maximum disc value of the other galaxies. That then results in a situation where NGC 3992 is substantially sub maximum while the other galaxies in the cluster are at maximum. Because NGC 3992 is barred one might have expected just the opposite and therefore this option is not likely. When the whole argumentation given above is considered, the conclusion has to be reached that the mass-to-light ratio of NGC 3992 is at least a factor of 1.35 larger than that of the average value of the UMa cluster.

This cannot be explained by a different stellar population. One then has to invoke a different IMF for NGC 3992, containing more low mass stars. But for that there is no obvious reason. The easy way out is, of course, by putting NGC 3992 and its companions at a larger distance and so behind the UMa cluster. To make the mass-to-light ratio a factor 1.35 (= 0.33 mag.) smaller, the NGC 3992 group needs to be 3.0 Mpc behind the cluster. For a factor 2.2 (= 0.86 mag.) lower M/L ratio the group should be 9 Mpc behind the cluster. Allowing a change in distance to NGC 3992 even makes it possible to create a larger contribution of the disc to the total rotation compared to the rest of the galaxies in the UMa cluster and thus solving some problems possibly associated with its barred morphology.

6.3. The Tully-Fisher relation

In Fig. 15 the I-band TF relation of Verheijen is reproduced. The maximum rotations of UGG 6923 and UGC 6969 have changed slightly because of the present study. The new values for these two galaxies have been put into the TF diagram of Fig. 15 and it should be noted that the triangle for UGC 6923 could have been replaced with a filled dot, meaning that the flat part of the rotation curve has been reached. Also the data point for UGC 6940 has been added to the diagram.

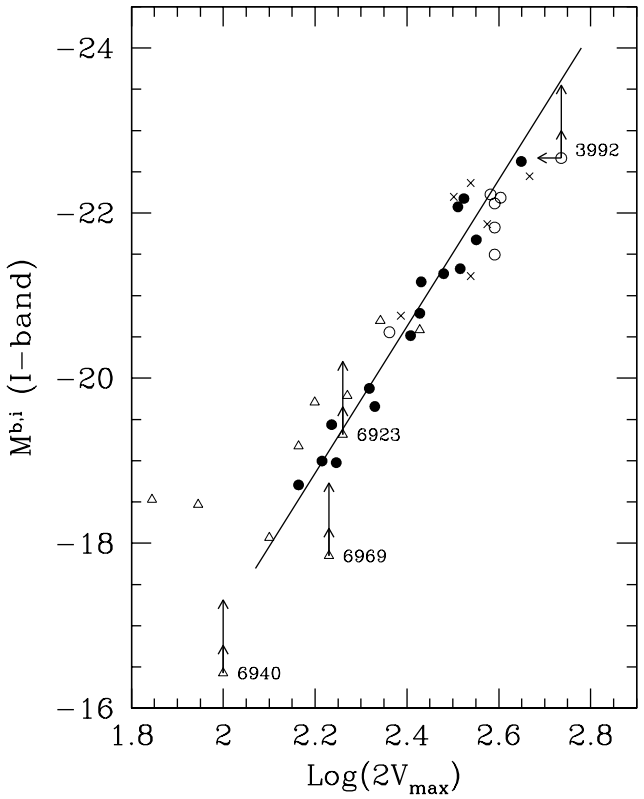

Fig. 15. Reproduction of Verheijens (1997) Tully-Fisher relation of the Ursa Major cluster. The data point for UGC 6940 has been added while the data points for UGC 6923 and UGC 6969 have been changed slightly according to the better determined maximum rotations ($V_{\rm max}$) in the present paper. The horizontal arrow attached to NGC 3992 indicates the shift when instead of the maximum rotation the flat part of the rotation curve is used. Vertical arrows indicate the increase in luminosity with 0.33 or 0.86 mag. caused by a larger distance of 3 or 9 Mpc respectively. The nearly equal rotation at different luminosities for UGC 6923 and UGC 6969 can be explained by different dark/luminous mass ratios for these galaxies.

Let us first discuss the position of NGC 3992 in the TF relation. It is obvious that NGC 3992 is too faint for its rotation, even if instead of the maximum rotation that of the flat part is taken. Doing the latter, NGC 3992 is 0.43 magnitude too faint. However, if the light of the galaxy would be increased by more than a factor 1.35 (> 0.33 mag.) the data point in the TF relation is consistent. If the different mass-to-light ratio of NGC 3992 is explained by a different IMF for that galaxy, only that data point in the TF relation has to be corrected. On the other hand, if a larger distance is needed all the four data points belonging to the NGC 3992 group in the relation (Fig. 15) have to be changed by 0.33 mag. (factor 1.35) or by 0.86 mag.

(factor 2.2). Considering Fig. 15, such shifts are certainly possible.

UGC 6923 and UGC 6969 have nearly the same maximum rotation, while differing a factor of five in luminosity. Yet, assuming a $(M/L)^i_I$ of 0.82 the dark halos of these two galaxies are identical to within the errors. This has an obvious effect on their position in the TF relation as can be seen in Fig. 15. The argument can now be turned around, the two galaxies have the same rotational velocity but differ by a factor of five in brightness because they have a different ratio of dark to luminous matter. A baryonic TF relation can be created (McGaugh et al. 2000) by also taking the gas mass of a galaxy into account. In general the scatter of the TF relation then seems to decrease for small galaxies. Using a fiducial gas M/L ratio of 0.82, the same as for the I-band rotation curve decomposition, the gas mass of UGC 6923 and UGC 6969 was converted into light. The difference in luminosity between the two galaxies then decreases to a factor $2\frac{1}{2}$, being still significant.

Except for the usual problems with absorption, populations effects, and inclination errors causing observational or semi-observational scatter in the TF relation there is also an intrinsic scatter, here twice illustrated by the NGC 3992 group. At first, small differences in M/L (already corrected for population effects and absorption) or in distance will cause data points to deviate. Secondly, different ratios of luminous to dark mass will obviously cause scatter. Matters are complicated because certainly for the smaller galaxies the maximum of the rotation is not reached at the end of the measured gas distribution. Considering all these problems it is not surprising that the TF relation can be applied to an individual case only with an appreciable error. For an ensemble of galaxies spanning a wide range of luminosities, the relation is a reflection of a globally equal ratio of dark to luminous matter.

7. Discussion and conclusions

This paper presents a nice example of two small galaxies which appear to have nearly equal dark matter halos. Yet one of the galaxies is considerably more luminous simply because it contains more luminous matter which is dominant in the inner regions. The other galaxy seems to be dominated by dark matter everywhere. As a hypothesis one could imagine a situation where different amounts of gas have fallen into the same halo, creating different amounts of stellar material. In any case, it is inevitable that a different formation scenario must have been at work, maybe associated with an interaction with the dominant galaxy NGC 3992.

For UGC 6969 the universal NFW halo does not apply. In general a more essential question is: what is the fraction of small galaxies for which NFW is impossible? If that fraction appears to be small, those galaxies may have formed under exceptional circumstances maybe involving large amounts of dissipational matter or strong tidal interactions. The CDM structure formation is then not in serious trouble.

In my opinion the size of the abovementioned fraction is still undetermined. This has to do with the inherent difficulty in measuring rotation curves of LSB galaxies. The H I observations of de Blok & McGaugh (1997) inevitably suffer from beam smearing but as demonstrated by Swaters et al. (2000) beam smearing is most associated with the smallest or close to edge-on galaxies. For the more favourable objects of de Blok & McGaugh the derived rotation curves give a good impression of the actual rotation even though the rotation curves were derived from the x,v diagrams only. It is, of course, better to use the full velocity field (as done in this paper) or to use Hα observations especially for the inner regions. Anyway, I expect these matters can, and will be resolved in the near future.

Finally a compilation of the main conclusions of this paper:

1. Detailed observations in the neutral hydrogen line have been made of the large barred spiral galaxy NGC 3992 and its three small companion galaxies, UGC 6923, UGC 6940, and UGC 6969.
2. In general the H I distribution of all galaxies is regular. NGC 3992 has a faint radial H I extension outside its stellar disc; contrary to the companions where there is an abrupt end to the H I gas distribution.
3. For the three companions rotation curves have been derived from their velocity fields.
4. UGC 6923 and UGC 6969 have nearly the same maximum rotation. Yet the shapes of the rotation curves are different which is likely related to the factor of five difference in luminosity of the two.
5. Assuming a reasonable M/L ratio for the three companions, a decomposition of the rotation curves generates nearly equal dark matter halos.
6. An NFW-CDMΛ dark halo is consistent with the observed rotation curve of UGC 6923 but <u>not</u> consistent with the rotation curve of UGC 6969.
7. A comparison has been made of the absorption corrected I-band M/L ratio of NGC 3992 and these ratios of other galaxies in the UMa cluster. From that it can be concluded that or, the M/L ratio of NGC 3992 has to be at least 1.35 times larger than the average ratio of the cluster galaxies, or, the NGC 3992 group is situated more than 3 Mpc behind the cluster.
8. This can also explain the position of NGC 3992 in the Tully-Fisher relation of the Ursa Major cluster, where NGC 3992 is approximately 0.43 magnitudes too faint for its rotation.

Acknowledgements. The observations presented in this paper were obtained with the Westerbork Synthesis Radio Telescope (WSRT) which is operated by the Netherlands Foundation for Research in Astronomy (NFRA). I thank Marc Verheijen for his help during the initial stages of the data reduction and for

intense discussions and useful remarks. The Kapteyn Institute is acknowledged for providing hospitality and support.

References

Begeman K. 1987, Ph. D. Thesis, University of Groningen
Begeman K. 1989, A&A, 223, 47
Bell E.F., & de Jong R.S. 2001, ApJ, 550, 212
Bosma A 1978, Ph. D. Thesis, University of Groningen
Bottema R. 1993, A&A, 275, 16
Bottema R. 1997, A&A, 328, 517
Bottema R., & Verheijen M.A.W. 2002, to appear in A&A (Paper I)
Bullock J.S., Kolatt T.S., Sigad Y., et al. 2001, MNRAS, 321, 559
Carignan C., & Freeman K.C. 1985, ApJ, 294, 494
Courteau S., & Rix H.W. 1999, ApJ, 513, 561
de Blok W.J.G., & McGaugh S.S. 1997, MNRAS, 290, 533
de Blok W.J.G., McGaugh S.S., Bosma A., & Rubin V.C. 2001, ApJ, 552, L23
Freedman W.F., Madore B.F., Gibson B.K., et al. 2001, ApJ, 553, 47
Giovanelli R., Haynes M.P., Herter T., et al. 1997, AJ, 113, 22
Gottesman S.T., Ball R., Hunter J.H., & Huntley J.M. 1984, ApJ, 286, 471
Jing Y.P. 2000, ApJ, 535, 30
Kalnajs A.J. 1983, in IAU Symp. 100, The internal kinematics of galaxies, ed. Athanassoula, E., (Reidel, Dordrecht), p87
Kent S.M. 1986, AJ, 91, 1301
McGaugh S.S., Schombert J.M., Bothun G.D., & de Blok W.J.G. 2000, ApJ, 533, L99
McGaugh S.S., de Blok W.J.G., & Rubin V.C. 2001, AJ, 122, 2381
Navarro J.F. 1998, astro-ph/9807084
Navarro J.F., Frenk C.S., & White S.D.M. 1996, ApJ, 462, 563
Navarro J.F., Frenk C.S., & White S.D.M. 1997, ApJ, 490, 493
Pickering T.E., Impey C.D., van Gorkom J.H., & Bothun G.D. 1997, AJ, 114, 1858
Sakai S., Mould J.R., Hughes S.M.G., et al. 2000, ApJ, 529, 698
Salucci P., Ashman K.M., & Persic M. 1991, ApJ, 379, 89
Sancisi R., & Allen R.J. 1978, A&A, 74, 73
Sandage A., & Tammann G.A. 1981, A Revised Shapley-Ames Catalog of Bright Galaxies, Carnegie Institute of Washington
Sellwood J.A., & Moore E.M. 1999, ApJ, 510, 125
Swaters R.A., Madore B.F., & Trewhella M. 2000, ApJ, 531, L107
Tully R.B., & Fisher J.R. 1977, A&A, 54, 661
Tully R.B., & Fouqué P. 1985, ApJS, 58, 67
Tully R.B., & Pierce M.J. 2000, ApJ, 533, 744
Tully R.B., & Verheijen M.A.W. 1997, ApJ, 484, 145
Tully R.B., Verheijen M.A.W., Pierce M.J., et al. 1996, AJ, 112, 2471
Tully R.B., Pierce M.J., Huang J-.S., et al. 1998, AJ, 115, 2264
van Albada T.S., Bahcall J.N., Begeman K., & Sancisi R. 1985, ApJ, 295, 305
van Albada T.S., & Sancisi R. 1986, Phil. Trans. R. Soc. London, Ser. A, 320, 447
van der Marel R.P., & Franx M. 1993, ApJ, 407, 525
Verheijen M.A.W. 1997, Ph. D. Thesis, University of Groningen
Verheijen M.A.W., & Sancisi R. 2001, A&A, 370, 765

Table 1. Observing parameters

Telescope	WSRT
Observing date	May 1997 to Sept. 1997
Duration of observation	4×12 h.
Number of interferometers	~ 27
Baselines (min-max-incr.)	36 - 2736 - 36 m.
Full res. beam (FWHM, $\alpha \times \delta$)	$14'' \times 18''$
FWHpower primary beam	$37'$
Rms (1σ) noise per channel	
full res.	1.96 K = 0.473 $M_\odot$pc^{-2}
res. = $30'' \times 30''$	0.55 K = 0.132 $M_\odot$pc^{-2}
Velocity central channel	1050 km s^{-1}
Bandwidth	5 MHz
Number of channels	64
Channel separation	16.6 km s^{-1}
Velocity resolution	33.3 km s^{-1}
Field centre (1950)	($11^{\rm h}$ $55^{\rm m}$ $07^{\rm s}$; $53^\circ 39' 18''$)
K-mJy conversion,	
equivalent of 1 mJy/beam	2.62 K (full res.)
	0.73 K (res. = $30''$)
Adopted distance	18.6 Mpc

Table 2. Galaxy parameters

NGC 3992		
Hubble type	SBb(rs)I	a
Brightness (in B)	10.86 mag.	b
Brightness (in I)	8.94 mag.	b
Opt. incl. ($q_0 = 0.11$)	57°	b
Opt. PA major axis	68°(= 248°)	b
PA major axis bar	37°	c
Deprojected bar length	150″	d
Scalelength	undef	
Total H I mass	5.9 10^9 $M_\odot$	d
21 cm cont. flux	43.2 mJy	d
UGC 6923		
Brightness (in B)	13.91 mag.	b
Brightness (in I)	12.36 mag.	b
Opt. incl. ($q_0 = 0.11$)	66°	b
Opt. PA major axis	354°	b
Scalelength (in I)	20.″9	b
Total H I mass	0.64 10^9 $M_\odot$	e
21 cm cont. flux	$<$ 2.6 mJy	b
UGC 6940		
Brightness (in B)	16.45 mag.	b
Brightness (in I)	15.44 mag.	b
Opt. incl. ($q_0 = 0.11$)	75°	b
Opt. PA major axis	135°	b
Scalelength (in I)	8.″52	b
Total H I mass	0.16 10^9 $M_\odot$	e
21 cm cont. flux	$<$ 1.3 mJy	b
UGC 6969		
Brightness (in B)	15.12 mag.	b
Brightness (in I)	14.04 mag.	b
Opt. incl. ($q_0 = 0.11$)	73°	b
Opt. PA major axis	330°	b
Scalelength (in I)	11.″65	b
Total H I mass	0.44 10^9 $M_\odot$	e
21 cm cont. flux	$<$ 3.8 mJy	b

a Sandage & Tammann (1981)
b Verheijen (1997)
c Measured from photograph
d Paper I
e This paper

Table 3. The rotation curve of UGC 6923

R (″)	$V_{\rm rot}$ (km s^{-1})	$\varepsilon_{\rm vrot}$ (km s^{-1})	R (″)	$V_{\rm rot}$ (km s^{-1})	$\varepsilon_{\rm vrot}$ (km s^{-1})
10	38.3	10.3	60	82.2	1.4
20	57.7	3.0	70	91.8	9.0
30	62.5	1.2	80	83.5	5.2
40	70.8	1.8	90	91.6	7.2
50	76.4	1.6			
Pos. of dynamical centre					
RA (1950)		$11^{\rm h}\ 54^{\rm m}\ 14.^{\rm s}2$			
Declination (1950)		53°26′20.″7			
$V_{\rm sys}$ (Hel.)		1066 ± 2 km s^{-1}			
Inclination		66° (Opt.)			
P.A.		343° ± 4°			

Table 4. The rotation curve of UGC 6940

R (″)	$V_{\rm rot}$ (km s^{-1})	$\varepsilon_{\rm vrot}$ (km s^{-1})	R (″)	$V_{\rm rot}$ (km s^{-1})	$\varepsilon_{\rm vrot}$ (km s^{-1})
10	19.4	2.4	30	41.9	3.5
20	33.0	2.0	40	49.9	3.0
Pos. of dynamical centre					
RA (1950)		$11^{\rm h}\ 55^{\rm m}\ 12.^{\rm s}6$			
Declination (1950)		53°30′45.″3			
$V_{\rm sys}$ (Hel.)		1107 ± 2 km s^{-1}			
Inclination		75° (Opt.)			
P.A.		315° (Opt.)			

Table 5. The rotation curve of UGC 6969

R (″)	$V_{\rm rot}$ (km s^{-1})	$\varepsilon_{\rm vrot}$ (km s^{-1})	R (″)	$V_{\rm rot}$ (km s^{-1})	$\varepsilon_{\rm vrot}$ (km s^{-1})
10	17.1	8	50	64.5	2.1
20	35.8	2	60	67.3	5.0
30	49.8	3.6	70	77.2	5.4
40	59.8	3.9	80	84.4	5.4
Pos. of dynamical centre					
RA (1950)		$11^{\rm h}\ 56^{\rm m}\ 12.^{\rm s}9$			
Declination (1950)		53°42′8.″6			
$V_{\rm sys}$ (Hel.)		1114 ± 2 km s^{-1}			
Inclination		73° (Opt.)			
P.A.		331° ± 2°			

Table 6. Rotation decompositions of the companions

UGC		6923	6940	6969
Incl. (°)		66	75	73
h_I (kpc)		1.88	0.77	1.05
Obs. light (10^9 $L^I_\odot$)		1.76	0.104	0.376
Gas mass, H I + He (10^9 $M_\odot$)		0.89	0.22	0.622
$(M/L)^{\rm obs}_I$ max disc	Iso	1.64 ± 0.23	1.6 ± 0.2	1.78 ± 0.4
$R_{\rm core}$ max disc (kpc)	Iso	5.3 ± 2.2	> 20	9.2 ± 5.2
$v_{\rm h}^{\rm max}$ max disc (km s^{-1})	Iso	124 ± 57	> 500	199 ± 114
$R_{\rm core}$ min disc (kpc)	Iso	1.39 ± 0.16	2.0 ± 0.2	2.93 ± 0.33
$v_{\rm h}^{\rm max}$ min disc (km s^{-1})	Iso	93 ± 13	73 ± 8	104 ± 13
$R_{\rm core}$ $(M/L)^i_I = 0.82$ (kpc)	Iso	2.24 ± 0.27	3.45 ± 0.4	4.24 ± 0.6
$v_{\rm h}^{\rm max}$ $(M/L)^i_I = 0.82$ (km s^{-1})	Iso	94 ± 13	97 ± 11	121 ± 19
R_s $(M/L)^i_I = 0.82$ (kpc)	NFW	3.7 ± 0.2		2.9 ± 0.5
$v_{\rm max}$ $(M/L)^i_I = 0.82$ (km s^{-1})	NFW	63 ± 3		53 ± 6
R_s $(M/L)^i_I = 0$ (kpc)	NFW	4.8 ± 0.15		3.25 ± 0.45
$v_{\rm max}$ $(M/L)^i_I = 0$ (km s^{-1})	NFW	77 ± 2		57 ± 6
R_s $(M/L)^i_I = 0.82$ (kpc)	NFW-3σ			8.4 ± 1.3
$v_{\rm max}$ $(M/L)^i_I = 0.82$ (km s^{-1})	NFW-3σ			66 ± 7

Table 7. Light and mass-to-light ratios

Galaxy	$L^{\rm obs}_I$ (10^9 $L_\odot$)	Incl. (°)	A^i_I (Eq. 8) (mag.)	A^i_I used (mag.)	L^i_I (10^9 $L_\odot$)	$(M/L)^i_I$ max disc ($M_\odot/L_\odot$)	Mass for $(M/L)^i_I = 0.82$ (10^9 $M_\odot$)	Mass max disc (10^9 $M_\odot$)	Mass best fit (10^9 $M_\odot$)
N3992	41.16	57	0.26	0.52	66.27	2.91	54.3	194.1	73.7
U6923	1.76	66	0.34	0	1.76	1.64	1.44	2.89	-
U6940	0.104	75	0.52	0	0.104	1.6	0.085	0.17	-
U6969	0.376	73	0.47	0	0.376	1.78	0.308	0.67	-